ARTICLE NO. 79-0290R

J80-053

20005
20015
60003

Numerical Analysis of Flowfields Generated by Accelerating Flames

J. Kurylo*
Lawrence Berkeley Lab., Berkeley, Calif.
H. A. Dwyer†
University of California, Davis, Calif.
and
A. K. Oppenheim‡
University of California, Berkeley, Calif.

A numerical technique is presented for the analysis of nonsteady flowfields generated by accelerating flames in gaseous media. The problem is formulated in Eulerian coordinates and the solution is based on the extension of the floating shock-fitting technique to all the discontinuities and their interactions occurring in the flowfield. Besides shock waves, the discontinuities taken into account thus far consist of contact surfaces, deflagration, and detonation fronts. The governing partial differential equations are integrated by the use of an explicit second-order accurate, finite-difference scheme, while special algorithms are introduced for the treatment of segments of the flowfield where the influence zones of discontinuities overlap. Actual interactions between them are treated by the polar intersection method. The technique is applied to the case of a steady flame experiencing an abrupt increase in burning speed, leading either to the establishment of a new steady flame flow system or to further acceleration culminated by the transition to detonation. A demarcation line between the two regimes of solutions, depending on the value of the initial burning speed and the magnitude of its abrupt increase, is established, and the physical validity of this criterion is corroborated by experimental evidence.

Introduction

THE ability to analyze flowfields generated by accelerating flames recently became of particular importance as a result of the concern over danger inherent in explosive clouds which can be formed in the case of accidental fuel spills.[1] Thus, the activity in this field of study became quite escalated as demonstrated, for example, by the significant number of papers presented at the last Combustion Symposium.[2-4]

Since detonation presents a much greater danger than a deflagration, the prominent problems in this field are concerned with the initiation of detonation and, in particular, the transition from deflagration to detonation. A numerical analysis of such a problem has been presented recently by Boni et al.[5] Their computations were based on the use of a finite-difference technique employing an artificial viscosity to handle large gradients associated with discontinuities occurring in the flowfield.

The potential for transition to detonation, under conditions modeling the unconfined character of an explosive cloud, has been explored experimentally by Dörge et al.[6] The test gas, usually a stoichiometric propane-air mixture maintained in a large rectangular enclosure, was ignited at the center of the floor to form a hemispherical flame. At a certain distance from the center, a hemispherical screen was placed, so that the flame passing through it acquired an increase in turbulent intensity augmenting its burning speed. The observed change in flame velocity has been correlated with the Reynolds number based on the velocity of the undisturbed flame and the mesh size of the screen. With the use of oxygen enriched air, the flame could be accelerated in this manner to such an extent that transition to detonation was eventually attained.

The objective of the work presented here is to reveal the gasdynamic properties of the nonsteady flowfields generated in such phenomena and thereby elucidate the conditions associated with the transition to detonation. Conventional numerical techniques exploiting the device of artificial viscosity, such as that used by Boni et al., could not be used for this purpose since they smooth out the discontinuities occurring in the flowfield and cannot, therefore, treat the sharp wave interactions that dominate the development of the process.

The numerical method presented here is, on the contrary, particularly suitable for the analysis of nonsteady flowfields containing internal discontinuities that are in the course of mutual interactions, since it is capable of retaining the sharp character of their jump conditions. Our algorithm is, in effect, an extension of the floating shock-fitting technique, developed by Moretti[7] and Salas[8] for the study of steady two-dimensional flowfields, to nonsteady one-dimensional flows.

Principles of Analysis

As revealed by extensive experimental evidence acquired over the last twenty years,[9-11] flames, in the course of acceleration, become more compact so that the power density of energy release is increased, providing the extra drive required for this purpose. Therefore, in the analysis such flames must be treated as discontinuous deflagration fronts. Moreover, in the course of transition to detonation many wave interaction processes take place, generating a great number of contact surfaces which have been observed to retain their sharp character over a considerable amount of time. Thus the influence of transport properties appears to be negligible in comparison to the gasdynamic effects of wave interactions.

Presented as Paper 79-0290 at the AIAA Aerospace Sciences Meeting, New Orleans, La., Jan. 15-17, 1979; submitted March 5, 1979; revision received Aug. 14, 1979. Copyright © American Institute of Aeronautics and Astronautics, Inc., 1979. All rights reserved. Reprints of this article may be ordered from AIAA Special Publications, 1290 Avenue of the Americas, New York, N.Y. 10019. Order by article No. at top of page. Member price $2.00 each, nonmember, $3.00 each. **Remittance must accompany order.**

Index categories: Combustion Stability, Ignition and Detonation; Computational Methods; Shock Waves and Detonations.

*Engineer. Member AIAA.
†Professor, Mechanical Engineering. Member AIAA.
‡Professor, Mechanical Engineering. Fellow AIAA.

Consequently, in the analysis presented here, the medium is assumed to be inviscid, while the sharp character of wave fronts and their interactions are carefully taken into account. The nonsteady flowfield under study is considered to be spatially one-dimensional but, within this constraint, the analysis is set to treat planar-, line-, and point-symmetrical cases. However, all the wave fronts are treated as locally planar. This inhibits the application of our technique to continuous flowfields involving large gradients in gasdynamic parameters, such as a decaying point- or line-symmetrical blast wave in the vicinity of the front, but makes it particularly suitable for flowfields generated by piston action, such as that provided by the flame.

Thus, the solution we seek consists of continuous segments of time-dependent essentially invisicd flowfields, bounded by discontinous wave fronts which are in the course of mutual interactions. In a finite-difference scheme, deflagrations prove to be particularly troublesome, since the large jump in density and particle velocity with which they are invariably associated leads to large oscillations whenever the initial state is not determined with sufficient precision. For this reason, the computational grid we use is allowed to move with the velocity of the deflagration so that its front always coincides with a grid point, thus eliminating completely the truncation error.

According to these principles, the continuous portions of the flowfield being studied are governed by the Euler equations of motion. These are expressed as:

$$f_t + g_x = k \tag{1}$$

where subscripts t and x denote partial differentials with respect to time and space, respectively, while

$$f = \begin{bmatrix} \rho x^j \\ u\rho x^j \\ e\rho x^j \end{bmatrix};\quad g = \begin{bmatrix} u\rho x^j \\ [u^2 + (p/\rho)]\rho x^j \\ u[e + (p/\rho)]\rho x^j \end{bmatrix};\quad k = \begin{bmatrix} 0 \\ jpx^{j-1} \\ 0 \end{bmatrix}$$

In the preceding, p, ρ, and u have the usual meaning of pressure, density, and particle velocity, respectively

$$e = \frac{1}{\gamma - 1}\frac{p}{\rho} + \frac{u^2}{2}$$

where $\gamma = \text{const}$, while

$$j \equiv d\ell nA / d\ell nx$$

where A is the frontal area at a radius x from the center. Accordingly, $j = 0$, 1, or 2 for planar, cylindrical, or spherical geometry, respectively, of the flowfield.

In order to adopt the equations to a moving grid, the independent variables are transformed so that

$$t = t, \quad \alpha = x - wt \tag{2}$$

where w is the rate of the grid's displacement.

The partial derivatives then become

$$(\ )_t = (\ )_t - [w + t(dw/dt)](\ )_\alpha \tag{3a}$$

while

$$(\ )_x = (\ )_\alpha \tag{3b}$$

All the variables of the problem are, at the same time, normalized by the introduction of the following nondimensional parameters:

$$T \equiv \frac{t}{x_o}\frac{p_a^{1/2}}{\rho_a^{1/2}};\quad X \equiv \frac{\alpha}{x_o};\quad P \equiv \frac{p}{p_a};\quad R \equiv \frac{\rho\alpha^j}{\rho_a x_o^j}$$

$$U \equiv \frac{u\rho\alpha^j}{p_a^{1/2}\rho_a^{1/2}x_o^j};\quad E \equiv \frac{1}{\gamma - 1}\frac{p\alpha^j}{p_a x_o^j} + \frac{\rho u^2\alpha^j}{2p_a x_o^j};\quad W \equiv \frac{w\rho_a^{1/2}}{p_a^{1/2}}$$

where subscript a denotes the ambient conditions, and subscript o marks the reference radius.

Under such circumstances, the governing equations acquire the following form:

$$F_T + H_X = K \tag{4}$$

where

$$H = G - \left(W + T\frac{dW}{dT}\right)F$$

while

$$F = \begin{bmatrix} R \\ U \\ E \end{bmatrix};\quad G = \begin{bmatrix} U \\ (U^2/R) + PX^j \\ (U/R)(E + PX^j) \end{bmatrix};\quad K = \begin{bmatrix} 0 \\ jPX^{j-1} \\ 0 \end{bmatrix}$$

In the computations these equations are used to determine, at each time step, the three components of vector F. The value of P is then determined from the definition of E, namely,

$$P = \left(E - \frac{U^2}{2R}\right)\frac{\gamma - 1}{X^j}$$

The continuous segments governed by the preceding equations are bounded by discontinuities involving finite jump conditions which are evaluated by the use of the Hugoniot relations. For shock fronts, the latter are expressed in terms of a constant γ, while for deflagration, proper allowance is made to take into account the change of γ from γ_u for the unburned medium to γ_b for the burned gas.[12,13] The detonation is treated as a shock followed by a deflagration.

Principles of Computation

The differential equations are integrated by the use of the MacCormack technique,[14] following the routine adopted by Dwyer et al.[15] This is an explicit, noncentered, second-order accurate, two-step, finite-difference scheme that consists of a predictor and a corrector step which, with reference to Eq. (4), have, respectively, the following form

$$\overline{F_i^{n+1}} = F_i^n - (H_{i+1}^n - H_i^n)\frac{\Delta T}{\Delta X} + K_{i+1/2}^n \Delta T \tag{5}$$

$$F_i^{n+1} = \frac{1}{2}\left[(F_i^n + \overline{F_i^{n+1}}) - (\overline{H_i^{n+1}} - \overline{H_{i-1}^{n+1}})\frac{\Delta T}{\Delta X} + \overline{K_{i-1/2}^{n+1}}\Delta T\right] \tag{6}$$

Within this scheme, the elementary gasdynamic discontinuities and their interactions were computed explicitly by means of a floating discontinuity technique developed especially for this purpose. The technique is capable of taking into account the jump conditions without employing any artificial viscosity either explicitly or implicitly. Its application is described here with respect to shocks, contact surfaces, and deflagrations, respectively. As already pointed out, detonations are considered to be shocks followed by deflagrations and, therefore, do not require a separate treatment.

Shock Fitting

The rudimentary aspects of a shock traversing a computational grid are depicted in Fig. 1. There are two

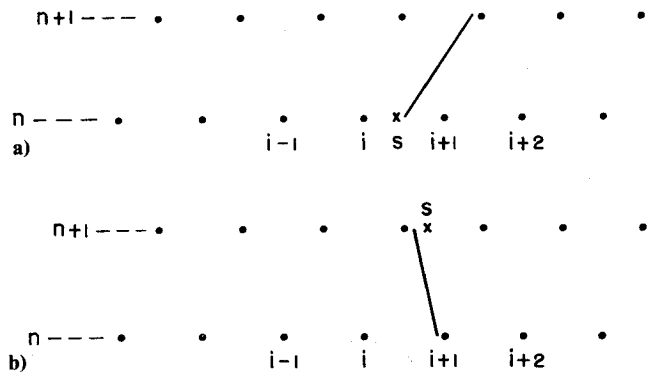

Fig. 1 Schematic diagram of shock traversing the computational grid: a) front propagating to the right; b) front propagating to the left.

possibilities: the shock can move to the right (case a) or to the left (case b). In the first case, a significant truncation error can occur in the predictor step of the MacCormack scheme; in the second, a similar error can arise in the corrector step. Both may lead to large instabilities. The difficulty is obviated by the use of a second-order approximation developed by Salas.[8] In effect, this involves an interpolation between grid points —taken in the first case at time (n) and, in the second, at time $(n+1)$—to take into account the exact position of the high-pressure state immediately behind the front. In Fig. 1 this is denoted by x located at an intermediate position s between grid points (i) and $(i+1)$.

The Salas modification affects only the middle term of the MacCormack scheme, namely, that involving the difference between the H's. These are then replaced as follows:[8,16]

$$(H^n_{i+1}-H^n_i) \Rightarrow \frac{2(2-\epsilon)}{1+\epsilon}H^n_s+(2\epsilon-3)H^n_i+\frac{(1-\epsilon)(2\epsilon-1)}{1+\epsilon}H^n_{i-1} \tag{7}$$

where

$$\epsilon=(X^n_s-X^n_i)/\Delta X$$

and

$$(H^{\overline{n+1}}_i-H^{\overline{n+1}}_{i-1}) \Rightarrow \frac{2(2-\epsilon)}{1+\epsilon}H^{\overline{n+1}}_s+(2\epsilon-3)H^{\overline{n+1}}_{i+1}+\frac{(1-\epsilon)(2\epsilon-1)}{1+\epsilon}H^{\overline{n+1}}_{i+2} \tag{8}$$

where

$$\epsilon=(X^{\overline{n+1}}_{i+1}-X^{\overline{n+1}}_s)/\Delta X$$

For the low-pressure side, computational stability is attained by reversing the foward differences in the predictor and backward differences in the corrector step.

A shock can traverse the computational grid in five different ways. These are shown in Fig. 2. Thick solid lines represent shock trajectories, thin lines with arrows pointing upward or downward are mnemonics indicating the direction in which the MacCormack predictor or corrector is applied at the node into which the arrow is pointing. Straight arrowhead lines point out the nodes where the predicted and corrected values of gasdynamic parameters behind the shock are related by the Rankine-Hugoniot jump conditions to the state immediately ahead of the front. Predicted values of these parameters are determined on the basis of the initial shock strength, while their corrected values are based on the average of the initial and predicted strengths.

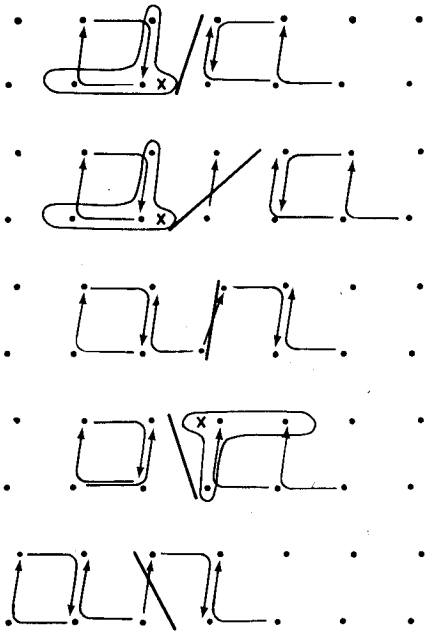

Fig. 2 Schematic diagrams of various ways in which a shock can traverse the computational grid.

The sets of computational points involved in the Salas modified algorithm are identified by showing them enclosed in kidney-shaped boundaries. Those embodying three parameters at time (n), as in the first two cases, are involved in the predictor step of Eq. (5) with the modification specified by Eq. (7) to evaluate conditions for a single point at time $(n+1)$. Those embodying three parameters at time $(n+1)$, as in the fourth case, are involved in the corrector step of Eq. (6) with the modification specified by Eq. (8).

It is of interest to note that the shock-fitting technique developed by Moretti,[7] utilizing the Rankine-Hugoniot relations and the information carried along the characteristics intersecting the shock on the high-pressure side, showed no advantage over the floating shock fitting. In fact, Salas[8] pointed out that the determination of the origin of the characteristic merging with the shock may become extremely difficult in the vicinity of other discontinuities.

Deflagration Fitting

As one of the principles of our analysis, the computational grid is made to move with the velocity of the deflagration so that its front always coincides with a node. Thus, the fitting of the deflagration as it traverses the computational grid is straightforward and unambiguous. There is only one way in which this can occur, as illustrated in Fig. 3. The trajectory of deflagration is represented there as a thick dashed line. Nodes (i) and $(i+1)$ coincide in space, but in computations they represent states immediately adjacent to the front on its two sides. Their parameters are related by the jump conditions across the deflagration.

The fitting of the deflagration is accomplished by combining the jump relations across it in the forward and backward direction with the MacCormack predictor and corrector steps, as indicated by the arrowheads in Fig. 3.

When the propagation speed of the deflagration is below the Chapman-Jouguet value, conditions behind it (node i on side b in Fig. 3) can influence those ahead (node $i+1$ on side u). To make matters worse, the burning law prescribing the deflagration speed, S_u, is usually expressed so that jump relations for each gasdynamic parameter cannot be expressed in a closed algebraic form. The evaluation of these relations requires, in this case, the use of an iterative procedure involving, besides the burning law, the mass, momentum, and the Hugoniot equations.

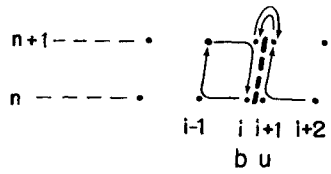

Fig. 3 Schematic diagram of a deflagration traversing the computational grid.

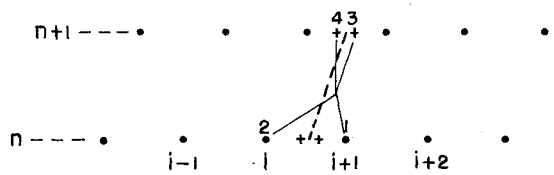

Fig. 4 Schematic diagram of a contact surface traversing the computational grid.

When the deflagration acquires the Chapman-Jouguet velocity, conditions behind it cannot influence those ahead and the jump relations for each parameter can be expressed in a closed algebraic form. The fitting procedure is then significantly simpler.

Contact Surface Fitting

Contact surfaces are formed by wave interactions. Their existence is intimately related to the dynamic compatibility condition governing the interaction process: the demand for the establishment of a regime of uniform pressure and particle velocity immediately behind two adjacent wave systems—a condition that, in general, gives rise to two regimes of different density and velocity of sound, separated by the contact surface. Since the difference between these parameters occurring across the surface can be quite large, failure to properly take them into account in a finite-difference scheme may lead to large oscillations.

For this reason, contact surfaces are treated with particular care. The computational technique we employ for this purpose utilizes the solution to the Riemann problem—the evaluation of a steady wave system associated with different gasdynamic conditions existing at two adjacent grid points. This is accomplished by the use of a rapidly converging iteration algorithm devised by Chorin.[17]

Rudimentary properties of a contact surface traversing a computational grid are displayed in Fig. 4, while all the possible ways in which this process can take place are presented in Fig. 5. On these diagrams the trajectory of the contact surface is depicted by a dashed line, the crosses mark the states immediately ahead and behind. The four thin lines in the immediate vicinity of the trajectory indicate exactly how the solution to the Riemann problem is applied. It is based on the values of the parameters at states 1 and 2, that is, at nodes $(i+1)$ and (i), and provide data for states 3 and 4 at the two intermediate points marked by crosses. These are then utilized in the Salas-modified algorithms, as indicated in Fig. 5, where the computational points involved in them are shown enclosed in boundaries of the same shape and corresponding meaning as those in Fig. 2.

It should be noted that the Salas algorithm permitted the predictor and corrector schemes to bypass the discontinuity in all the cases except for the last one. However, here it turned out that ascribing the values of parameters at state 3 to the closest node matched well with the MacCormack corrector and did not cause any problem.

Multidiscontinuity Fitting

In Figs. 2, 3, and 5 all of the grid points connected by lines with arrowheads are involved in the fitting procedure for the single discontinuities they display. These grid points in effect constitute their zones of influence. If there are two or more discontinuities whose zones of influence intersect, the fitting

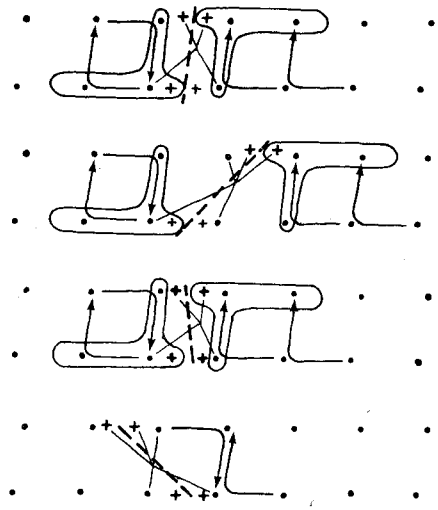

Fig. 5 Schematic diagrams of various ways in which a contact surface can traverse the computational grid.

procedure involves iterations across the full extent of these zones. This requires special handling—a task which is accomplished by the use of appropriate subroutines. For this purpose, we developed algorithms to treat a number of double as well as multiple discontinuity systems.

The set for double discontinuity systems includes the following cases: 1) shock-shock, 2) shock-deflagration, 3) shock-contact surface, and 4) deflagration-contact surface. The latter three involve two subroutines to cover the different situations incurred depending on the side from which one discontinuity encounters the other.

The set of triple discontinuity systems consists of: 1) shock-contact surface-shock, 2) shock-contact surface-deflagration, and 3) contact surface-deflagration-shock. Moreover, we had to include a subroutine for a case involving four discontinuities; namely, 4) shock-contact surface-deflagration-shock.

The subroutines for multidiscontinuity systems are made out of those for double discontinuity systems by including proper procedures for matching the parameters at grid points shared by their zones of influence.

Interactions

When the trajectories of discontinuities within intersecting influence zones are converging, they eventually interact with each other. In conformity with the major assumption of negligible viscous effects we adopted, such interactions are considered to occur instantaneously. Moreover, the participating discontinuities are treated as locally planar. Consequently, the solution of an interaction process is obtained by invoking the principle of the dynamic compatibility condition according to which the resulting wave system can create only a regime of uniform pressure and particle velocity. As already pointed out, it is this condition that gives rise to a contact surface.

The computations are based on the concept of wave polar—the locus of all possible end states behind a given discontinuity in the plane of pressure and particle velocity. In order to satisfy the dynamic compatibility condition, wave polars for all the discontinuities participating in an interaction process must form a closed contour.[12,18]

The interactions are treated accordingly by appropriate subroutines. These include: 1) generation of shocks by a deflagration undergoing a finite increment in propagation speed, 2) shock merging with a deflagration, 3) shock merging with a shock, 4) shock colliding with a shock, 5) shock colliding with a contact surface across which the velocity of sound increases, 6) shock colliding with a contact surface

across which the velocity of sound decreases, and 7) deflagration colliding with a contact surface.

Methodology of Application

The procedure we adopted for computation follows. First, the time-step is evaluated by the Courant-Friedrichs-Lewy stability condition, assuring that the numerical domain of dependence at every point in the flowfield includes that of the set of hyperbolic partial differential equations governing the solution. Gasdynamic parameters for all the grid points of the flowfield at the next time interval are then computed by applying the MacCormack predictor-corrector scheme as if there were no discontinuities involved in the problem. The discontinuities present in the flowfield are then located and their type identified. Thereupon, by the use of appropriate subroutines employing the floating fitting technique, the motion of the discontinuities and the flowfields around them are determined.

This is continued until the influence zones of the discontinuities start to intersect. At that time a check is made of the adequacy of separation from other discontinuities that may be present in the flowfield. If this test fails, an additional check is made to find out whether one has to treat a triple or a quadruple discontinuity system. Having established the type of multiple discontinuity system encountered, the proper subroutine is invoked and the computations are continued until the trajectories of the discontinuities tend to interact within the next time interval.

Thereupon, the interaction is computed by the appropriate subroutine using the wave polar method. In the course of interactions taking place in the burned medium, the strength of shock waves and contact surfaces is checked. Shocks whose Mach number is less than 1.001 and contact surfaces across which the density changes by less than 2% are discarded.

Numerical Example

The numerical example illustrating the application of our technique concerns an accelerating flame in a typical hydrocarbon-air mixture close to stoichiometric composition. Its thermodynamic properties are expressed as follows:

Specific volume ratio at an initial pressure:	$\nu_F = 7$
Specific heat ratio of unburned medium:	$\gamma_u = 1.3$
Specific heat ratio of burned gases:	$\gamma_b = 1.2$
Ambient pressure:	$p_a = 1$ atm
Velocity of sound at ambient conditions:	$a_a = 331$ m/s

The flame burning speed is expressed in terms of a law based on ample experimental evidence[19-23], namely,

$$S_u = S_o (p_u/p_a)^{0.5} (a_u/a_a)^{4.6}$$

where subscript o denotes the initial flame speed, and subscripts a and u refer, respectively, to conditions of the ambient atmosphere into which the flame propagates initially and to those immediately ahead of its front.

Initial conditions for the computations are provided by the solution of the pressure wave generated by a flame propagating with constant burning speed, S_o.[13]

When the flame is at a radius $X = 1$, its speed is suddenly increased by a finite increment ΔS. The ensuing development of the process is determined using our computational technique.

A time-space wave diagram of the solution is presented in Fig. 6. Here we had $S_o = 9.6$ m/s, and $\Delta S = 14.6$ m/s, while the flow was considered to be plane symmetrical ($j = 0$). A solution obtained under similar circumstances for the same initial flame speed but with $\Delta S = 19.0$ m/s is displayed in Fig. 7. On both diagrams, dashed thick lines represent the trajectories of deflagrations, solid lines refer to shocks, the thick solid line corresponds to detonation, and the thin broken lines indicate the particle paths.

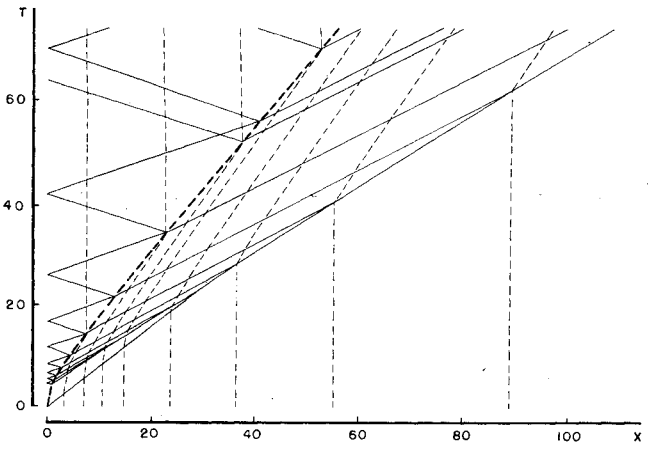

Fig. 6 Wave diagram of stable solution obtained in the case of subcritical burning speed increment.

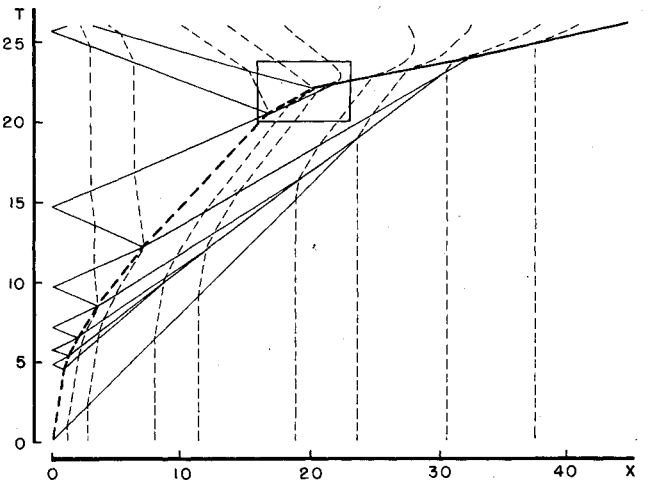

Fig. 7 Wave diagram of unstable solution obtained in the case of supercritical burning speed increment.

In the first case, the imploding shock, generated when the flame speed was suddenly increased at $x = x_o$, was reduced to a sound wave after eight reflections from the center and interactions with the deflagration. In the meantime, the propagation speed of the deflagration increased to 37.2 m/s, while the Mach number of the shock at the front of the pressure wave was augmented from 1.1 to 1.4. The process took about 240 x_o ms while the deflagration traveled a distance of 53 x_o m, where x_o is expressed in meters. Thereupon the whole wave system settled to a steady state corresponding to a self-similar solution obtained for the final propagation speed of the deflagration.

In the second case, however, as demonstrated in Fig. 7, the process escalated to detonation propagating finally at a speed of 2250 m/s. Its onset occurred at a radius of 20.3 x_o m and the time of 76 x_o ms. Associated with this was the generation of a retonation wave traveling at a speed of 1250 m/s, corresponding to a local Mach number of 1.29, into the burned medium.

Details of the wave interaction processes associated with the onset of the detonation and retonation waves are shown in Fig. 8. This is, in effect, an enlargement of a part of the solution delineated by a small rectangle on Fig. 7. Added here for clarity of exposition are the characteristics. As it appears here, the onset of detonation is also associated with the formation of a centered rarefaction wave. Its front edge is at the Chapman-Jouguet state propagating with the detonation front, while its trailing edge is identified on the diagram by a chain-double-dotted line.

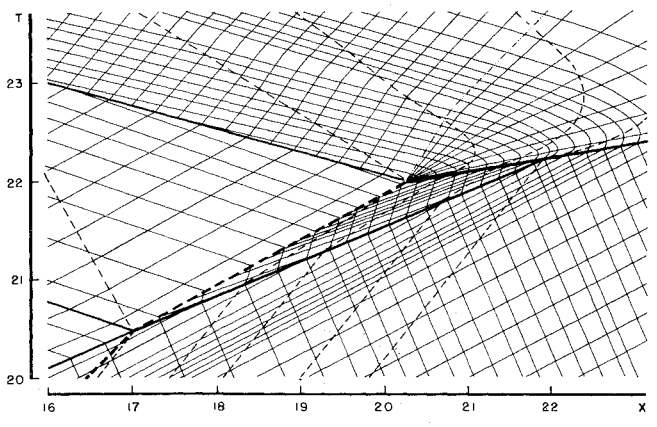

Fig. 8 Details of solution presented in Fig. 7 depicting the onset of detonation.

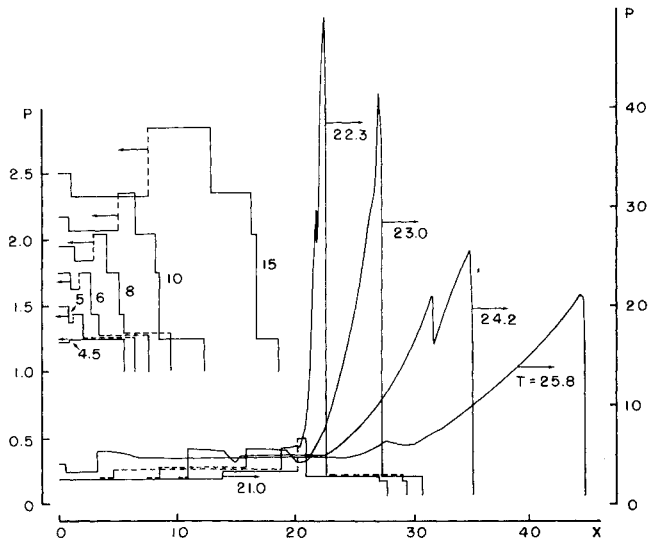

Fig. 9 Pressure space profiles at various instants obtained with the solution presented by Fig. 7.

The evolution of pressure profiles corresponding to the solution presented in Figs. 7 and 8 is displayed in Fig. 9. For early times, they are presented in a larger scale on the left side; for later times, they are in a smaller scale on the right. The earliest is that for $T=4.5$ showing the pressure distribution prior to the increment in the burning speed of the flame. The pressure profiles from then on until $T=15$ demonstrate the remarkable ability of our technique in tracing sharp jumps associated with shocks without exhibiting any diffusional effect or any computational instabilities. The profile at $T=22.3$ exhibits the effects of the centered rarefaction wave generated at the onset of detonation. Soon thereafter, at $T=25$, the pressure profile acquires the familiar shape of a self-similar blast wave headed by a Chapman-Jouguet detonation.

Thus, there are two possibilities: a steady solution culminated by a constant velocity flame driving a pressure wave or an unsteady solution associated with transition to detonation. The distribution between the two is governed solely by the value of the initial flame speed and the flame speed increment. The demarcation line between the two regimes of these parameters is presented in Fig. 10. For initial conditions corresponding to a point below the line, stable solution, like that of Fig. 8, is obtained; for points above the line, the solutions are unstable, as exemplified by Fig. 7.

For the stable case, similar solutions as that of Fig. 6 were obtained by our Cloud Code[24]—a Lagrangian computational

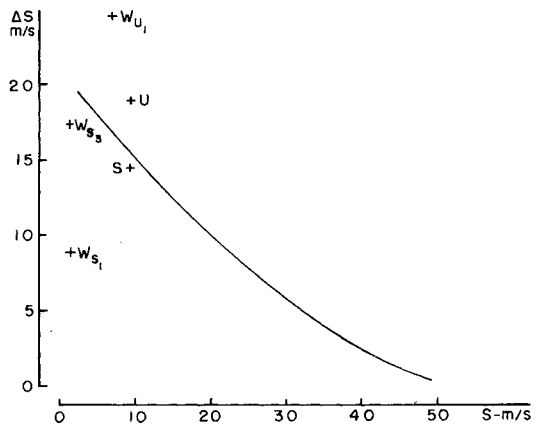

Fig. 10 Regimes of initial conditions for stable and unstable solutions.

scheme for blast waves employing the von Neumann-Richtmyer artificial viscosity with Wilkins' modification. When the unstable conditions associated with transition to detonation were approached, however, the computations became excessively unstable. This feature manifested itself so distinctly that it was actually exploited to check the demarcation line of Fig. 10. With the use of the Cloud Code, such lines were determined for spherical as well as planar flowfields. The difference between them turned out to be so small that the line presented in Fig. 10 could be considered to be valid irrespectively of the geometry of the flowfield.

Noted on the diagram are a number of specific points marked by crosses. That indicated by S corresponds to the solution of Fig. 6; the point denoted by U specifies initial conditions for the solution presented in Figs. 7-9. Points indicated by W refer to experimental results obtained by Dörge et al.[6] with the use of acetylene-air mixtures. Subscript S denotes cases when the flame, after passing the screen barrier, settled to a new steady propagation velocity. Subscript U refers to the unstable case associated with transition to detonation, which was observed when air was enriched with oxygen. The numerals in the subscripts indicate the number of turbulence-generating screens used in the experiment. As it appears, the increase in flame-burning speed could be practically doubled by the use of three screens instead of one. However, the addition of oxygen to the air was evidently so effective in augmenting the flame speed increment that one screen was, in this case, quite sufficient.

Conclusions

Presented herein is a numerical technique capable of treating sharply all the discontinuous wave fronts and their interactions occurring in a nonsteady flowfield, such as that generated by an accelerating flame in the course of transition to detonation. The results obtained by its use are devoid of the effects of numerical diffusion and are thus instrumental in revealing the details of the gasdynamic phenomena governing the mechanism of the development of detonation.

In the example used to illustrate the application of the technique—a constant velocity flame undergoing a sudden increase in its burning speed—a line of demarcation has been established between the regime of stable solutions whose final state is that of a constant velocity flame driving a self-similar blast wave, and that of unstable solutions characterized by the transition to detonation. The physical significance of this concept, as well as the actual position of the demarcation line on the plane of the initial flame speed and its increment, have been corroborated by experimental evidence. One should note in this connection that the burning speed and its increment express in effect all the chemical kinetic and transport properties of the medium that play an essential role in the transition to detonation.

The example has a weak point: the law adopted to describe the dependence of the flame-burning speed on the conditions immediately ahead of its front is too rudimentary. The flame speed has been expressed as a function of only the thermodynamic state, while, in reality, one would expect a significant dependence on the local scale and intensity of turbulence. Since in a given flow system both are functions of the freestream velocity, one would have $S_u = S(p,T,u_u)$ while the form used in the example is restricted to $S_u = S(p,T)$.

In this respect, the following should be noted:

1) The computational technique we present is capable of handling any law governing the flame-burning speed.

2) We have not been able to find specific information in the literature on the dependence of propagating flames on the turbulence in the unburned medium.

3) As a consequence of the restriction imposed by continuity, the particle velocity ahead of the flame is *de facto* accounted in its burning speed. If, for example, $u_b = 0$ then $u_u = (\nu_F - 1)S_u$. Since in a nonsteady flowfield, local particle velocity is functionally related to pressure and temperature, one is thus left with $S_u = S(p,T)$, as actually used in our calculations.

4) The flame-burning speed governs the flow only at the initial stages of flame acceleration. In the case of transition to detonation, which has been of primary interest in the development of our technique, the deflagration acquires quite rapidly the Chapman – Jouguet condition, whereupon the process becomes independent of the flame speed law.

5) In accordance with the preceding, the results we obtained are in satisfactory agreement with experimental observations.

Acknowledgment

This work was supported by the Army Research Office under Grant DAAG-29-77-G-0064 and the Department of Energy under Contract No. W-7405-ENG-48. The authors wish to express their appreciation to J. H. Lee whose comments were extremely helpful in improving the quality of the exposition.

References

[1] Strehlow, R. A., "Unconfined Vapor Cloud Explosions—An Overview," *Fourteenth Symposium (International) on Combustion*, The Combustion Institute, Pittsburgh, Pa., 1973, pp. 1189-1200.

[2] Knystautas, R., Lee, J. H., Moen, I., and Wagner, H. Gg., "Direct Iniation of Spherical Detonation by a Hot Turbulent Gas Jet," *17th Symposium (International) on Combustion*, The Combustion Institute, Pittsburgh, Pa., 1978, pp. 1235-1245.

[3] Brossard, J., Perrot, J., and Manson, N., "Pressure Waves Generated by Detonating Spherical Gaseous Charges," *Seventeenth Symposium (International) on Combustion*, The Combustion Institute, Pittsburgh, Pa., 1978.

[4] Nicholls, J. A., Sichel, M., and Gabrijel, Z., "Detonability of Unconfined Natural Gas-Air Clouds," *17th Symposium (International) on Combustion*, The Combustion Institute, Pittsburgh, Pa., 1978, pp. 1223-1233.

[5] Boni, A. A., Wilson, C. W., Chapman, M., and Cook, J.L., "A Study of Detonation in Methane/Air Clouds," *Acta Astronautica*, Vol. 5, Issue 11/12, 1978, pp. 1153-1169.

[6] Dörge, K. J., Pangritz, D., and Wagner, H. Gg., "Experiments on Velocity Augmentation of Spherical Flames by Grids," *Acta Astronautica*, Vol. 3, Issue 11/12, 1976, pp. 1067-1076.

[7] Moretti, G., "Thoughts and Afterthoughts About Shock Computations," Polytechnic Institute of Brooklyn, PIBAL Rept. 73-37, Dec. 1972.

[8] Salas, M. D., "Shock Fitting Method for Complicated Two-Dimensional Supersonic Flows," *AIAA Journal*, Vol. 14, May 1976, pp. 583-588.

[9] Lee, J. H., Soloukhin, R. I., and Oppenheim, A. K., "Current Views on Gaseous Detonation," *Acta Astronautica*, Vol. 14, No. 5, 1969, pp. 565-584.

[10] Oppenheim, A. K. and Soloukhin, R. I., "Experiments in Gasdynamics of Explosions," *Annual Review of Fluid Mechanics*, Vol. 5, 1973, pp. 31-58.

[11] Oppenheim, A. K. and Kamel, M. M., *Laser Cinemtography of Expolsions*, Springer-Verlag, Wien, New York, 1972.

[12] Oppenheim, A. K., *Introduction to Gasdynamics of Explosions*, Springer-Verlag, Wien, New York, 1972.

[13] Kuhl, A. L., Kamel, M. M., and Oppenheim, A. K., "Pressure Waves Generated by Steady Flames," *Fourteenth Symposium (International) on Combustion*, The Combustion Institute, Pittsburgh, Pa., 1973, pp. 1201-1215.

[14] MacCormack, R. W., "The Effect of Viscosity in Hypervelocity Impact Cratering," AIAA Paper 69-354, 1969.

[15] Dwyer, H., Allen, R., Ward, M., Karnopp, D., and Margolis, D., "Shock Capturing Finite Difference Methods for Unsteady Gas Transfer," AIAA Paper 74-521, 1974.

[16] Salas, M. D., private communication, 1976.

[17] Chorin, A. J., "Random Choice Solution of Hyperbolic Systems," *Journal of Computational Physics*, Vol. 22, Dec. 1976, pp. 517-533.

[18] Shapiro, A. H., *The Dynamics and Thermodynamics of Compressible Fluid Flow*, Vol. 1, The Ronald Press Co., New York, 1973.

[19] Gilbert, M., "The Influence of Pressure on Flame Speed," *Sixth Symposium (International) on Combustion*, Reinhold Publishing Corp., New York, 1957, pp. 74-83.

[20] Goldenberg, S. A. and Pelevin, V. S., "Influence of Pressure on Rate of Flame Propagation in Turbulent Flow," *Seventh Symposium (International) on Combustion*, The Combustion Institute, Pittsburgh, Pa., 1959, pp. 590-594.

[21] Bradley, D. and Hundy, G. F., "Burning Velocity of Methane-Air Mixtures Using Hot-Wire Anemometers in Closed-Vessel Explosions," *Thirteenth Symposium (International) on Combustion*, The Combustion Institute, Pittsburgh, Pa., 1971, pp. 573-583.

[22] Andrews, G. E. and Bradley, D., "The Burning Velocity of Methane-Air Mixtures," *Combustion and Flame*, Vol. 19, No. 2, 1972, pp. 275-288.

[23] Andrews, G. E. and Bradley, D., "Determination of Burning Velocity by Double Ignition in a Closed Vessel," *Combustion and Flame*, Vol. 20, No. 1, 1973, pp. 77-89.

[24] Cohen, L. M., Short, J. M., and Oppenheim, A. K., "A Computational Technique for the Evaluation of Dynamic Effects of Exothermic Reactions," *Combustion and Flame*, Vol. 24, No. 3, 1975, pp. 319-334.